applied sciences

MDPI

Article

Influence of Process Parameters on the Hydrothermal Carbonization of Olive Tree Trimmings: A ^{13}C Solid-State NMR Study

Lucia Calucci and Claudia Forte *

Istituto di Chimica dei Composti OrganoMetallici—ICCOM, Consiglio Nazionale delle Ricerche—CNR, Via G. Moruzzi 1, 56124 Pisa, Italy

* Correspondence: claudia.forte@pi.iccom.cnr.it

Abstract: Chars obtained from the hydrothermal carbonization (HTC) of agricultural wastes are increasingly being employed as solid biofuels. Their properties are strongly dependent on HTC process parameters. In this study, ^{13}C solid-state NMR spectroscopy was applied to semiquantitatively investigate carbon functionalities present in olive tree trimming feedstock and in the corresponding hydrochar samples. Hydrochars were obtained by HTC under different conditions, that is, at two different temperatures (180 and 250 °C), with two different biomass/water ratios (B/W of 7 and 25% *w*/*w*) and with reaction times at peak temperatures of 30, 60, and 180 min. The NMR analysis was complemented by infrared spectroscopy experiments. A detailed analysis of carbon functionalities and their evolution during HTC allowed the transformation of feedstock into hydrochar to be followed and the structure of hydrochars to be correlated to the different reactions occurring during HTC in dependence on reaction time, temperature, and B/W ratio, as well as to the hydrochar properties fundamental for their application as solid biofuel reported in previous studies. ^{13}C solid-state NMR spectroscopy revealed a powerful tool for explaining hydrochar properties as a function of HTC parameters.

Keywords: HTC; infrared spectroscopy; ^{13}C CP MAS; cellulose; hemicellulose; lignin

Citation: Calucci, L.; Forte, C. Influence of Process Parameters on the Hydrothermal Carbonization of Olive Tree Trimmings: A ^{13}C Solid-State NMR Study. *Appl. Sci.* **2023**, *13*, 1515. https://doi.org/10.3390/app13031515

Academic Editors: Ana M. L. Seca and Serge Lavoie

Received: 20 December 2022
Revised: 14 January 2023
Accepted: 20 January 2023
Published: 24 January 2023

1. Introduction

Hydrothermal carbonization (HTC) is a thermochemical process that can be used to convert fresh biomass into valuable carbon-rich materials, generally referred to as hydrochars [1]. In recent years, with the increasing attention towards environmentally friendly processes and renewable energy sources, HTC has attracted much interest given the low energy consumption of the process and the possible application of hydrochars as solid fuels. In fact, HTC is carried out at relatively low temperatures (180–250 °C) and under water pressure; hence, it is possible to use wet biomass without a preliminary energy-consuming drying process [2]. Moreover, hydrochars have a much higher calorific value than the initial biomass [3,4]. Relevant to the use of hydrochars as fuel is, among other parameters, the higher heating value (HHV), which is related to char composition, and, combined with the mass yield of the process, determines the energy yield. In general, higher fixed carbon content, HHV and degree of aromatization render carbon materials more apt to replace fossil carbon sources.

The structure and properties of chars produced by HTC depend on process parameters, such as the highest temperature reached, the residence time at the peak temperature, and the solid load expressed as the biomass-to-water ratio (B/W), with an interplay between the different parameters [4,5]. Temperature has been found to determine the degree of carbonization, the calorific value, and mass yield, the first two increasing and the latter decreasing with increasing temperature [6]. The residence time has been observed to have a similar effect, although less pronounced [4,7]. In general, higher energy yields are obtained

in milder conditions (i.e., temperature < 230 °C and residence time ≤ 6 h) since, under more severe conditions, the HHV does not significantly increase, whereas the mass yield decreases [8]. Contrasting results are reported in the literature regarding the effects of the B/W ratio. HHV and mass yield were found to decrease with decreasing B/W [6], but in other cases the opposite trend in mass yield was observed [9]. Also feedstock type affects the HTC process. In fact, although all biomass mainly consists of the same three components, i.e., lignin, cellulose, and hemicellulose, in variable proportions, the interactions between lignin (less prone to degradation) and the other two components may alter their degradation pathway and kinetics [4]. Less important is the inorganic content since, due to dissolution in water, ashes in hydrochars are typically much less than in the initial feedstock. The low ash content represents an added value since it reduces the possibility of fouling, slagging, and corrosion during the combustion process [3,10].

Given the issues related to organic waste management, the application of HTC to biomass from municipal, industrial, or agricultural wastes has been extensively investigated [4,11]. Among the agricultural wastes investigated, olive tree trimmings, widely available in Mediterranean countries, have been recently studied [6,12–16]. Olive pruning contains about 31–35% of water and therefore it is suitable for HTC, whereas it would require a drying step if pyrolysis, gasification or torrefaction were used. All studies have demonstrated the good energy densification of olive tree pruning hydrochar.

For a thorough physico-chemical characterization of hydrochars, several instrumental techniques and analytical methods have been used, and among them ^{13}C solid-state Nuclear Magnetic Resonance (SSNMR) spectroscopy has revealed to be of great relevance [5,17–21]. Indeed, this technique allows carbon functionalities of complex organic matrices, such as feedstocks and chars, to be (semi)quantitatively determined on whole samples, irrespective of their crystalline or amorphous nature, and without requiring any sample pretreatment.

The overall purpose of this study was to investigate the effects of the different hydrothermal carbonization process parameters on the chemical structure of olive tree trimming hydrochars in order to discern the chemical transformations of the biomass during HTC and to highlight the relationships between atomic-scale properties and the macroscopic parameters of relevance for the application of hydrochar as a fuel. To this end, the structure of chars produced by HTC at different temperatures (180 °C and 250 °C), for different reaction times (from 30 to 180 min), and with different biomass/water ratios (B/W equal to 7 and 25% w/w) was investigated employing ^{13}C SSNMR spectroscopy, complemented by Fourier Transform infrared (FTIR) spectroscopy. A careful analysis of the spectroscopic data was performed, and the semiquantitative information obtained on carbon functionalities was discussed in relation to the reactions occurring in different HTC conditions and to fuel properties, such as HHV and fixed carbon content.

2. Materials and Methods

2.1. Samples

Feedstock and hydrochar samples were available from previous studies [6,12,13]. In particular, the feedstock consisted of olive tree trimmings, leaves included, from three 30-year-old trees of the Moresca variety. After drying in an oven at 40 °C for 48 h to eliminate the excess moisture, the trimmings were ground to a particle size <2 mm and sieved. Before the HTC tests, the feedstock was dried in an oven at 105 °C for 12 h. After adding the appropriate amount of water to the dried feedstock to reach the desired biomass/water (B/W) ratio, HTC was performed, following the procedure reported in previous studies [6,12,13]. B/W of 7 and 25% w/w were used, and the reaction times at peak temperature were set to 30, 60, or 180 min. The reaction temperature was 250 °C for all samples but one, where it was 180 °C. Hydrochar samples were dried in a ventilated oven at 105 °C until constant weight. Samples are indicated as FS (feedstock) and HTC_B/W_T_t, where B/W is either 7 or 25, T is the reaction temperature (°C), and t is the reaction time (min).

2.2. Infrared Spectroscopy

Infrared spectra were recorded using a Perkin-Elmer Spectrum One FTIR Spectrophotometer using KBr pellets. Spectra were acquired over the 4000–400 cm^{-1} range, with a spectral resolution of 4 cm^{-1} and accumulating 128 scans.

2.3. ^{13}C SSNMR Spectroscopy

^{13}C magic angle spinning (MAS) NMR spectra were recorded on a Bruker AVANCE spectrometer equipped with a 4 mm CP-MAS probe head operating at 400.13 MHz for proton and 100.62 MHz for carbon-13. ^{1}H-^{13}C cross-polarization (CP) spectra with proton dipolar decoupling were recorded on all samples, using a contact time of 2 ms, a recycle delay of 8 s and acquiring 1200 scans; the RF field strength was 71.5 kHz for both CP and dipolar decoupling. Preliminary tests were performed to find the experimental parameters that allowed a higher overall S/N ratio to be obtained. All spectra were recorded at room temperature with a MAS rate of 8 kHz. In some cases, spectra were also acquired at different MAS rates to assess the possible presence of spinning sidebands in the spectra. The chemical shifts were referenced to TMS using adamantane as external standard.

For a site-specific quantification of the different functional groups, deconvolution of the CP-MAS spectra was performed using the SPORT-NMR software [22]. The relative signal integral intensities obtained from the deconvolution were used for a semiquantitative estimation of the relative abundances of the different C functional groups over the following chemical shift regions: 0 to 45 ppm (alkyl C), 45 to 60 ppm (methoxyl and N-alkyl C), 60 to 110 ppm (O-alkyl and di-O-alkyl C), 110 to 145 ppm (H-, C-substituted aromatic C and furanic C), 145 to 165 ppm (O-substituted aromatic C and furanic C), 165 to 190 ppm (carboxyl C), and 190–220 ppm (aldehyde and ketone C). The area of signals over each spectral region was then expressed as a percentage of the total spectral area [23].

3. Results

3.1. FTIR Spectroscopy

The FTIR spectra of the feedstock (FS) and char samples after HTC in different conditions are reported in Figure 1. The FS spectrum (Figure 1a) showed features typical of lignocellulosic materials, with peaks mainly arising from functional groups in carbohydrates, i.e., cellulose and hemicellulose, and lignin [18,24–34]. The bands in the 3000–2800 cm^{-1} region and the broad band between 3700 and 3100 cm^{-1} were ascribable to asymmetric and symmetric C-H stretching vibrations in methyl and methylene groups and to the O-H stretching vibrations in hydroxyl and carboxyl groups, respectively. These functional groups are present in both carbohydrates and lignin, while cutin, suberin, and extractives containing methylene and methyl groups may contribute to the bands between 3000 and 2800 cm^{-1} [24]. Bands from carbohydrates were observed at 1732, 1375, 1210, 1165, 1060, and 1033 cm^{-1}, ascribable to C=O, C-H, C-O-C, and C-O deformation and stretching vibrations of different groups. In particular, the band at 1732 cm^{-1} was assigned to C=O stretching vibrations of the carboxyl and acetyl groups in hemicellulose. Moreover, the bands at 1318 and 895 cm^{-1} arise from the CH_2 rocking and the C-H deformation in cellulose, while the band at 1375 cm^{-1} is assigned to C-H deformation in cellulose and hemicellulose. Bands ascribable to aromatic C=C and C-O stretching and bending vibrations of different lignin groups were detected at 1610, 1512, and 1265 cm^{-1}, while signals arising from aromatic C-H deformations were found between 900 and 700 cm^{-1}. Bands from C-H and C-O deformation, bending, and stretching vibrations of groups in carbohydrates and lignin were observed at 1457, 1430, and 1110 cm^{-1}.

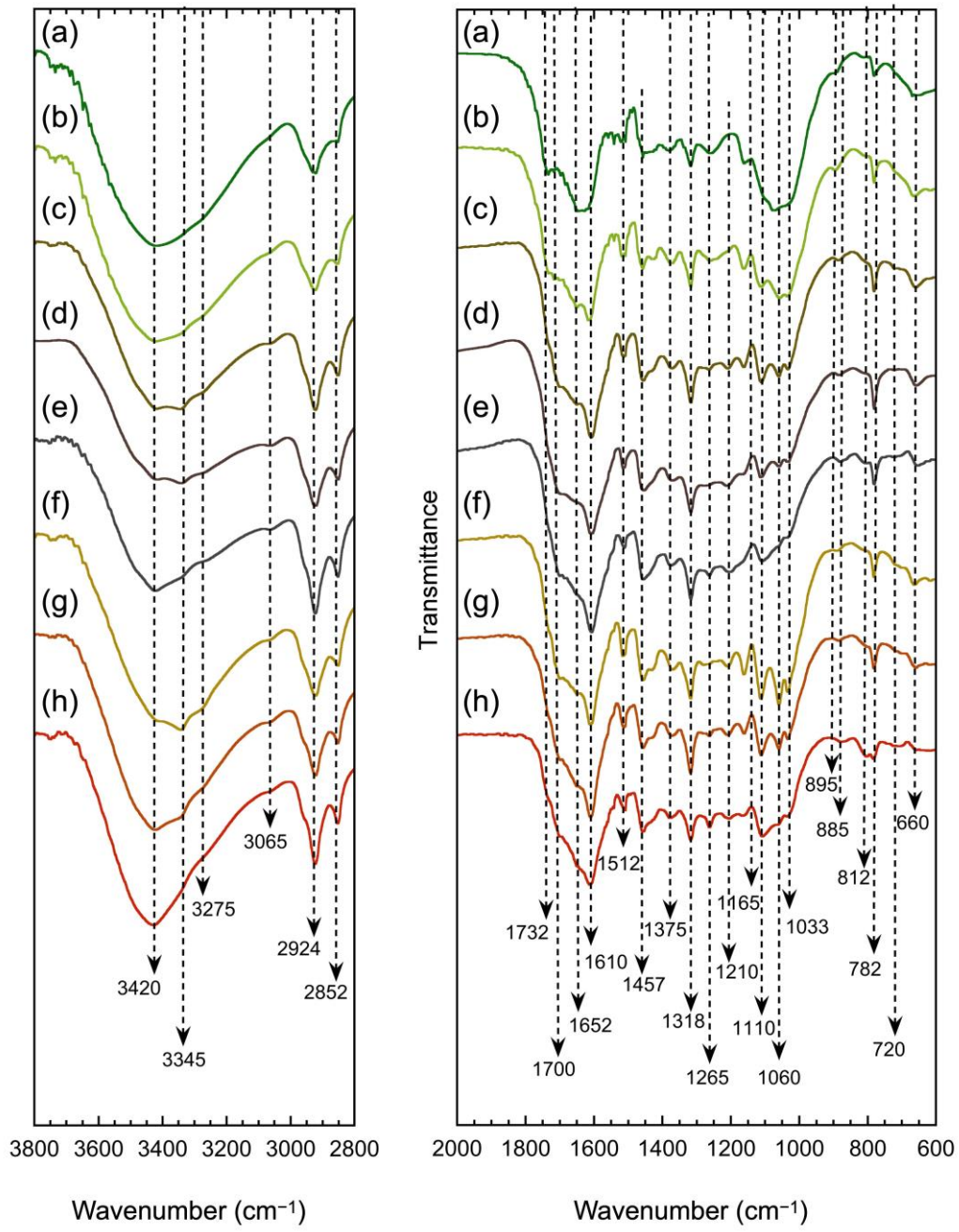

Figure 1. FTIR spectra of FS (**a**) and hydrochar samples HTC_25_180_30 (**b**), HTC_25_250_30 (**c**), HTC_25_250_60 (**d**), HTC_25_250_180 (**e**), HTC_7_250_30 (**f**), HTC_7_250_60 (**g**), and HTC_7_250_180 (**h**).

Upon HTC treatment, several changes occurred in the FTIR spectra (Figure 1b–h), associated with the transformation of olive trimming components during the carbonization process [5,14,18,24,26–28,30–33,35–38]. The broad O-H stretching, observable in the spectra of all hydrochars, showed a decrease in intensity with increasing treatment time for samples with B/W = 25% *w*/*w* and a reaction temperature of 250 °C; at the same time, the band maximum shifted to higher wavenumbers. On the other hand, this band was not affected by HTC at 180 °C, while the treatment at 250 °C for samples with B/W = 7% *w*/*w* only caused the band shift. A band at 3065 cm^{-1} due to aromatic C-H stretching vibration was visible in the hydrochar spectra, although with very low intensity. The alkyl C-H stretching signals in the 3000–2800 cm^{-1} region slightly increased in intensity with increasing treatment time and temperature. The band of hemicellulose at 1732 cm^{-1}, clearly distinguishable in the

feedstock, remained visible after HTC at 180 °C, whereas it appeared as a shoulder of the adjacent C=O stretching bands at 1700 and 1652 cm^{-1} upon treatment at 250 °C. The latter bands showed a significant increase in intensity with increasing treatment temperature, while they initially increased and then decreased again with increasing treatment time. The aromatic or furanic C=C and C=O stretching bands at 1610, 1512 and 1427 cm^{-1}, hardly visible in the feedstock spectrum, increased upon treatment at 180 °C and 250 °C for 30 min, remaining almost constant for longer treatments. Of the aliphatic C-H deformation bands, mainly due to cellulose, the CH and CH_2 ones significantly increased with treatment, the former (at 1457 cm^{-1}) remaining practically constant after the initial increase, the latter (at 1318 cm^{-1}) progressively increasing. Conversely, the CH_2 band at 1375 cm^{-1} did not change upon treatment. The bands at 1265 and 1210 cm^{-1}, due to aromatic C-O and phenolic O-H, respectively, were more clearly visible upon treatment. Lignin O-CH_3 groups mainly contributed to the band at 1265 cm^{-1}; the observation of this band in all hydrochar samples indicates the preservation of lignin during treatment [32]. The band at 1165 cm^{-1}, ascribed to C-O-C in carbohydrates, decreased for longer treatment times. The aliphatic C-O-C stretching band at 1110 cm^{-1} increased with treatment temperature but decreased at long treatment times. From an initially broader band, distinct bands at 1060 and 1033 cm^{-1} appeared upon treatment at 250 °C, decreasing at long reaction times. The small band at 895 cm^{-1} due to cellulose, present in the FS spectrum, disappeared upon HTC treatment. The presence of aromatic structures in the thermally treated samples was also indicated by the signals at 885, 812, and 782 cm^{-1}, ascribable to out-of-plane C-H bending in aromatic rings.

3.2. ^{13}C SSNMR Spectroscopy

For a more detailed characterization of the chemical structure of our materials, feedstock and hydrochar samples were investigated by ^{13}C CP-MAS NMR. In agreement with FTIR, the NMR spectrum of FS (Figure 2a) presented the characteristic signals of lignocellulosic materials [18,39–42]. In particular, the 60–110 ppm spectral region was dominated by the signals of cellulose [43], with less intense signals deriving from hemicellulose (C-1 to C-6 carbons) [39] and from aliphatic side chains of lignin [44–48]. Indeed, cellulose signals are expected at 104.5 ppm for carbon C-1 of β-D-glucose units, at 72.1 and 74.6 ppm for C-2, C-3, and C-5, at 83.3 and 88.1 ppm for C-4, and at 62.2 and 64.5 ppm for C-6. The signals at 88.1 and 64.5 ppm, due to C-4 and C-6 of crystalline or internal cellulose, and those at 83.3 and 62.2 ppm, due to amorphous cellulose and cellulose on the surface of fibers, were not clearly distinguished due to the higher intensity of the broader amorphous signals. The shoulder at about 102 ppm was ascribed to amorphous cellulose or hemicellulose C-1. The signal of carboxyl carbons from acetate groups of hemicellulose was observed at 172.5 ppm [41,43,49]. Conversely, the signal of acetate methyl carbons was not clearly distinguished at 21.0 ppm, due to the superposition with signals of other alkyl groups in the 0–45 ppm region, arising from carbohydrates and lignin, but also from organic extractives, cutin, and suberin [5]. In particular, the strong signal at about 30 ppm is typical of long aliphatic chains. Aromatic lignin carbons, resonating between 115 and 160 ppm [44–48] (in particular, protonated aromatic carbons between 115 and 128 ppm and oxygen-bonded aromatic carbons between 147 and 160 ppm) could be observed, even though their signals had low relative intensity. The methoxyl group signal typical of lignin was detected at 55.7 ppm [39].

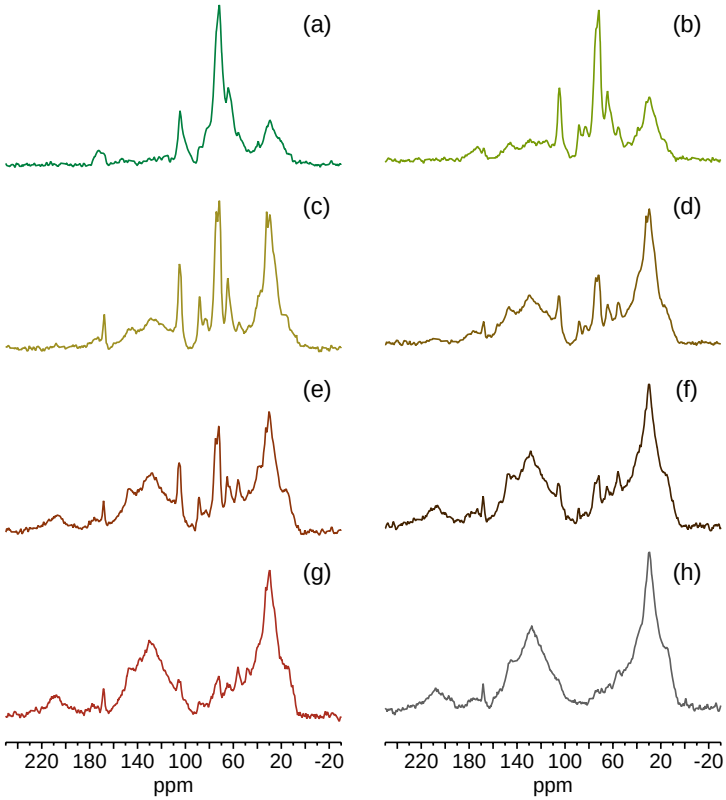

Figure 2. ^{13}C CP-MAS NMR spectra of FS (**a**) and hydrochar samples HTC_25_180_30 (**b**), HTC_7_250_30 (**c**), HTC_25_250_30 (**d**), HTC_7_250_60 (**e**), HTC_25_250_60 (**f**), HTC_7_250_180 (**g**), and HTC_25_250_180 (**h**).

The ^{13}C CP-MAS NMR spectra of the hydrochars obtained from the different treatments are shown in Figure 2b–h. Three main changes were observed in the spectra of the carbonized samples as temperature and reaction time increased: (1) The carbohydrate signals (in the 60–110 ppm spectral region) became narrower and decreased in intensity; (2) The relative intensities of alkyl (0–45 ppm) and aromatic C (110–165 ppm) signals increased; (3) New signals appeared due to carboxyl (165–190 ppm) and carbonyl (190–220 ppm) functional groups. In fact, after HTC at 180 °C (Figure 2b), the narrowing of the signals in the 60–110 ppm region, mainly due to cellulose and hemicellulose, indicated a significant reduction in the contribution of amorphous cellulose and hemicellulose compared to crystalline cellulose. The broad signals of the amorphous components strongly decreased for the hydrochars obtained at 250 °C, as highlighted by the narrow linewidth of the carbohydrate signals, even after 30 min of treatment (Figure 2c,d). The latter signals decreased in intensity as treatment time increased (Figure 2c–h). However, cellulose was not completely transformed even at the longest reaction time, and a slower decreasing trend was observed when HTC was performed with a lower B/W ratio (B/W = 7% *w*/*w* *vs.* B/W = 25% *w*/*w*) (Figure 2g,h). Also the signal of residual lignin at ~56 ppm was observable in all the hydrochar spectra. New signals appeared in the aliphatic (0–45 ppm) and aromatic (110–165 ppm) regions, as well as in the carboxyl (165–190 ppm) and carbonyl (190–220 ppm) regions, due to the formation of new chemical structures. In particular, a sharp signal at 168.0 ppm was observed in the spectra of all hydrochars produced at 250 °C (Figure 2c–h), ascribable to inorganic carbonates [50]. The formation of carbonyl groups, mainly ketones, was clearly observed for treatment times ≥60 min (Figure 2e,h). This finding agrees with results reported in the literature on HTC of carbohydrate-based materials [18,19,21,51–53].

A more detailed and quantitative description of the transformation of organic matter during the different HTC processes could be obtained by performing a deconvolution of the

^{13}C CP-MAS NMR spectra. The procedure was first applied to the FS spectrum (Figure 2a) to analyze signals from the different feedstock components in detail. The deconvolution of the hydrochar spectra (Figure 2b–h) was performed, keeping the chemical shift values of the feedstock signals fixed and using the minimum number of additional signals required to achieve a good reproduction of the experimental spectra. In the aliphatic region of the hydrochar spectra, the main contributions were found at 41, 36, 30, 26, and 17 ppm, some of them already present in the FS spectrum, increasing in intensity with treatment time and temperature. In the region between 110 and 165 ppm, signals at 110, 120, 125, 129, 132, 139, and 144 ppm were found, in addition to those of lignin at ~147 and 153 ppm and signals with lower intensity at 149 and 158 ppm. The additional signals can be ascribed to aromatic and furanic structures formed during HTC by the transformation of carbohydrates, while the signal at 110 ppm can be ascribed to furan units. Those at 125 and 132 ppm are assigned to arene units and those at 147–152 ppm to both arene and furan units [51,52]. Based on the relative intensities of these signals, the aromatic structures were found to prevail over the furanic ones for all hydrochar samples. The integral intensities of the signals obtained from the spectral deconvolutions were therefore determined over the seven spectral regions indicated in the Materials and Methods section. The relative intensities are reported in Figure 3.

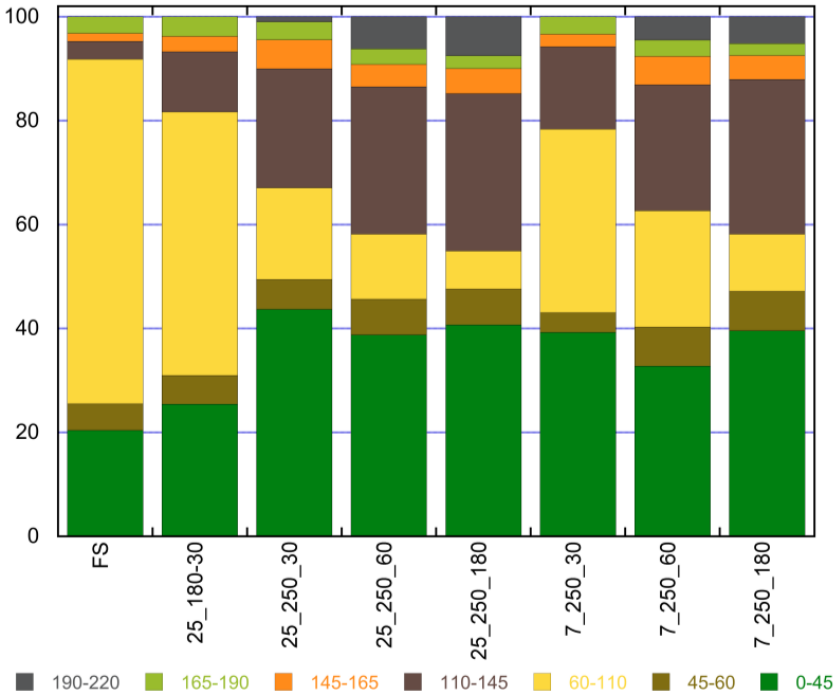

Figure 3. Relative integral intensities of signals in the indicated spectral regions of ^{13}C CP-MAS NMR spectra of FS and hydrochar samples.

As can be observed from Figure 3, carbohydrates, mainly responsible for the intensity in the 60–110 ppm region, are the main component of olive tree trimmings, and they are only partially decomposed during HTC, the decomposition being more severe when the process is conducted at higher temperature, higher solid load, and for more extended periods. In the HTC process alkyl and aromatic structures are formed, which add to those already present in the feedstock due to recalcitrant waxes, cutin, suberin, and lignin. As a result, aromatic components progressively increase by increasing HTC temperature, time, and B/W ratio, whereas allyl components increase by increasing HTC temperature and B/W ratio but do not show a clear trend with reaction time. The lignin O-CH_3 signal between 45 and 60 ppm is present in all spectra, confirming lignin recalcitrance to hydrothermal carbonization. The contribution of carboxyl structures decreases by prolonging the HTC

process, whereas an opposite trend is observed for carbonyl groups, the formation of which is observed only after treatment at 250 °C and is favoured by the higher solid load.

4. Discussion

The effects of the process parameters temperature, treatment time, and biomass/water ratio on the structure of hydrochars obtained by HTC of olive tree trimmings was qualitatively investigated by FTIR spectroscopy, then studied in more detail and more quantitatively by ^{13}C SSNMR spectroscopy. The differences observed in the FTIR spectra recorded on hydrochar samples with respect to that of the feedstock (Figure 1) can be explained in terms of the reactions known to occur during the HTC process [2–4]. In particular, dehydration and decarboxylation reactions can be associated with the loss of intensity of the O-H stretching band between 3700 and 3000 cm^{-1} and bands of carbonyl and alcohol groups in the "fingerprint region", with both reactions being favoured at higher treatment temperature, longer heating times, and higher B/W ratio. These reactions mainly occur on carbohydrate components, as indicated by the evolution of the bands at 1732 cm^{-1} (from hemicellulose), 895 cm^{-1} (from cellulose) and 1165 cm^{-1}, whereas lignin seems to remain almost unreacted after HTC in the adopted conditions. On the other hand, aliphatic alkyl structures, aromatic and furanic units, and carbonyl functional groups increase in content during the HTC process, as indicated by the bands at 3000–2800 cm^{-1} (alkyl chains), 3065, 1610, 1512, 1527, 885–782 cm^{-1} (aromatic structures), 1265 and 1210 cm^{-1} (C-O and phenolic O-H), and 1700 and 1652 cm^{-1} (C=O groups).

A more detailed picture of the transformations occurring during HTC was achieved from the ^{13}C CP-MAS NMR spectra (Figures 2 and 3). The first effect of HTC at lower temperatures and short carbonization time is the hydrolysis of hemicellulose and amorphous cellulose [54], as shown by the narrowing of carbohydrate signals in the 60–110 ppm region. Indeed, in previous studies, extractives and hemicellulose were found to be easily hydrolysed and completely solubilized in hot compressed water, with the consequent presence of monomers and oligomers in the liquid aqueous phase [1–4,55,56]. Moreover, part of the amorphous cellulose and soluble lignin is fragmented into smaller molecules, mainly into oligosaccharides and 5-hydroxymethylfurfural the former, into phenolic derivatives the latter [7]. On the contrary, crystalline cellulose was found to be resistant to hydrolysis, as expected for a lignocellulosic biomass, where cellulose may be protected from water by lignin and by hemicellulose.

By increasing the temperature and prolonging the HTC treatment, cellulose is also transformed, as indicated by the decrease in intensity of the O-alkyl and di-O-alkyl signals in the 60–110 ppm region. In fact, at temperatures >230 °C, subcritical water can disrupt the hydrogen bonds and crystalline structure of cellulose, hydrolysing the β-(1-4)-glycosidic bonds to form glucose monomers [1]. Nonetheless, carbohydrate components are still detected in the ^{13}C CP-MAS NMR spectra of hydrochars at the longest HTC reaction time of 180 min, even for those obtained with the lower B/W ratio.

The solubilization and hydrolysis products are generally highly reactive, undergoing condensation, oligomerization and polymerization reactions. These reactions occur in parallel [1,3,4], ultimately leading to the formation of polymeric furanic and aromatic structures connected by aliphatic chains. The solid residue formed through these reactions is often called secondary char. These reactions may be accompanied by dehydration, decarboxylation, and decarbonylation reactions. When precipitates form on the surface of cellulose, water access is inhibited. Consequently, cellulose is subject to pyrolysis and not dissolution and hydrolysis [57], giving carbonaceous materials with aromatic structures instead of furanic ones [58]. Additional contributions to the aromatic structures arise from lignin. Indeed, soluble lignin fragments are quickly polymerized. Moreover, some stable lignin crystalline structures may undergo demethylation and pyrolytic reactions without fragmentation [1]. As a result, minor chemical and physical modifications occur to lignin during the HTC process, especially under mild conditions [32,59]. The interconnected network formed by non-dissolved pyrolyzed cellulose and lignin is usually referred to as

primary char. The aliphatic structures increase upon HTC treatment. This trend indicates, on one side, the recalcitrance to hydrolysis of aliphatic structures present in waxes, cutin, and suberin and, on the other, the formation of new alkyl groups from the dehydration of the alkoxy ones [49,60].

On the whole, the HTC treatment in the mild conditions reported here gives rise only to a partial carbonization of the feedstock, as previously observed for different biomasses [5,18,21,35,61,62]. The transformation from a lignocellulosic composition to a mainly aromatic network, typically observed for biomasses upon HTC at much higher temperatures [31,32], only partially occurred during the HTC processes carried out here. The biomass load (B/W = 25% *w*/*w vs*. B/W = 7% *w*/*w*) mainly affects the decomposition and carbonization rates which are higher for the higher B/W ratio (Figure 3).

Our spectroscopic data (Figures 2 and 3) indicate that hydrochars are constituted of hydrophobic aromatic/aliphatic structures, but are also rich in reactive oxygen functional groups (i.e., hydroxyl/phenol, carboxyl, or carbonyl). Moreover, aromatic structures prevail over furanic ones, and residual feedstock components (mainly lignin) are conserved in the hydrochar samples. The obtained results can help to explain some properties of hydrochars from lignocellulosic biowaste at the molecular level and the HTC mechanisms reported in previous studies [6,12,13]. The increase in carbon content and decrease in oxygen content observed by increasing the HTC temperature (from 180 to 250 °C) and reaction time (from 30 to 180 min) is strongly correlated to the progressive carbonization of carbohydrates by dehydration and decarboxylation reactions, as well as to the preservation of lignin and alkyl components. The prevalence of aromatic over furanic structures suggests that primary char is mainly formed under the explored HTC conditions, in agreement with ref. [13,21]. The structures detected by the NMR experiments are also compatible with the higher HHV, energy densification ratio (EDR), and fixed carbon found for hydrochar samples obtained at higher temperatures after longer treatments [6,12,13].

As far as the effect of solid load on hydrochar properties is concerned, the lower carbonization degree of carbohydrates observed at the lower B/W ratio agrees with the lower carbon increase and oxygen decrease found by ultimate analysis and with the lower HHV, EDR, and fixed carbon values reported in ref. [6]. Indeed, at lower biomass load, the greater capacity of the liquid phase to dissolve molecular fragments arising from biomass hydrolysis, as observed by the higher liquid mass yield [6], hinders the polymerization and condensation reactions leading to the formation of secondary char.

Author Contributions: Conceptualization, L.C. and C.F.; methodology, L.C. and C.F.; software, L.C. and C.F.; validation, L.C. and C.F.; formal analysis, L.C.; investigation, L.C. and C.F.; data curation, L.C. and C.F.; writing—original draft preparation, L.C. and C.F.; writing—review and editing, L.C. and C.F.; supervision, L.C. and C.F. All authors have read and agreed to the published version of the manuscript.

Funding: This research received no external funding.

Data Availability Statement: The data presented in this study are available on request from the corresponding author.

Acknowledgments: L. Fiori and M. Volpe are kindly acknowledged for providing the feedstock and hydrochar samples.

Conflicts of Interest: The authors declare no conflict of interest.

References

1. Funke, A.; Ziegler, F. Hydrothermal carbonization of biomass: A summary and discussion of chemical mechanisms for process engineering. *Biofuels Bioprod. Biorefin.* **2010**, *4*, 160–177. [CrossRef]
2. Kambo, H.S.; Dutta, A. A comparative review of biochar and hydrochar in terms of production, physico-chemical properties and applications. *Renew. Sustain. Energy Rev.* **2015**, *45*, 359–378. [CrossRef]
3. Fang, J.; Zhan, L.; Ok, Y.S.; Gao, B. Minireview of potential applications of hydrochar derived from hydrothermal carbonization of biomass. *J. Ind. Eng. Chem.* **2018**, *57*, 15–21. [CrossRef]

4. Wang, T.; Zhai, Y.; Zhu, Y.; Li, C.; Zeng, G. A review of the hydrothermal carbonization of biomass waste for hydrochar formation: Process conditions, fundamentals, and physicochemical properties. *Renew. Sustain. Energy Rev.* **2018**, *90*, 223–247. [CrossRef]
5. Zhu, X.; Liu, Y.; Qian, F.; Zhang, S.; Chen, J. Investigation on the physical and chemical properties of hydrochar and its derived pyrolysis char for their potential application: Influence of hydrothermal carbonization conditions. *Energy Fuels* **2015**, *29*, 5222–5230. [CrossRef]
6. Volpe, M.; Fiori, L. From olive waste to solid biofuel through hydrothermal carbonization: The role of temperature and solid load on secondary char formation and hydrochar energy properties. *J. Anal. Appl. Pyrolysis* **2017**, *124*, 63–72. [CrossRef]
7. Ulbrich, M.; Preßl, D.; Fendt, S.; Gaderer, M.; Spliethoff, H. Impact of HTC reaction conditions on the hydrochar properties and CO_2 gasification properties of spent grains. *Fuel Process. Technol.* **2017**, *167*, 663–669. [CrossRef]
8. Diakité, M.; Paul, A.; Jäger, C.; Pielert, J.; Mumme, J. Chemical and morphological changes in hydrochars derived from microcrystalline cellulose and investigated by chromatographic, spectroscopic and adsorption techniques. *Bioresour. Technol.* **2013**, *150*, 98–105. [CrossRef] [PubMed]
9. Sermyagina, E.; Saari, J.; Kaikko, J.; Vakkilainen, E. Hydrothermal carbonization of coniferous biomass: Effect of process parameters on mass and energy yields. *J. Anal. Appl. Pyrolysis* **2015**, *113*, 551–556. [CrossRef]
10. Reza, M.T.; Lynam, J.G.; Coronella, C.J. Hydrothermal carbonization: Fate of inorganics. *Biomass Bioenergy* **2013**, *49*, 86–94. [CrossRef]
11. Cavali, M.; Libardi, N., Jr.; de Sena, J.D.; Woiciechowski, A.L.; Soccol, C.R.; Filho, P.B.; Bayard, R.; Benbelkacem, H.; de Castilhos, A.B., Jr. A review on hydrothermal carbonization of potential biomass wastes, characterization and environmental applications of hydrochar, and biorefinery perspectives of the process. *Sci. Total Environ.* **2023**, *857*, 159627. [CrossRef] [PubMed]
12. Volpe, M.; Fiori, L.; Volpe, R.; Messineo, A. Upgrading olive trimmings residue as biofuel by hydrothermal carbonization and torrefaction: A comparative study. *Chem. Eng. Trans.* **2016**, *50*, 13–18. [CrossRef]
13. Lucian, M.; Volpe, M.; Fiori, L. Hydrothermal carbonization kinetics of lignocellulosic agro-wastes: Experimental data and modeling. *Energies* **2019**, *12*, 516. [CrossRef]
14. González-Arias, J.; Sánchez, M.E.; Martínez, E.J.; Covalski, C.; Alonso-Simón, A.; González, R.; Cara-Jiménez, J. Hydrothermal carbonization of olive tree pruning as a sustainable way for improving biomass energy potential. Effect of reaction parameters on fuel properties. *Processes* **2020**, *8*, 1201. [CrossRef]
15. Duman, G.; Balmuk, G.; Cay, H.; Kantarli, I.C.; Yanik, J. Comparative evaluation of torrefaction and hydrothermal carbonization: Effect on fuel properties and combustion behavior of agricultural wastes. *Energy Fuels* **2020**, *34*, 11175–11185. [CrossRef]
16. Gonzáles-Arias, J.; Baena-Moreno, F.M.; Sánchez, M.E.; Cara-Jiménez, J. Optimizing hydrothermal carbonization of olive tree pruning: A techno-economic analysis based on experimental results. *Sci. Total Environ.* **2021**, *784*, 147169. [CrossRef]
17. Cao, X.; Pignatello, J.J.; Li, Y.; Lattao, C.; Chappell, M.A.; Chen, N.; Miller, L.F.; Mao, J. Characterization of wood chars produced at different temperatures using advanced solid-state ^{13}C NMR spectroscopic techniques. *Energy Fuels* **2012**, *26*, 5983–5991. [CrossRef]
18. Calucci, L.; Rasse, D.; Forte, C. Solid-state nuclear magnetic resonance characterization of chars obtained from hydrothermal carbonization of corncob and Miscanthus. *Energy Fuels* **2013**, *27*, 303–309. [CrossRef]
19. Baccile, N.; Falco, C.; Titirici, M.-M. Characterization of biomass and its derived char using ^{13}C-solid state nuclear magnetic resonance. *Green Chem.* **2014**, *16*, 4839–4869. [CrossRef]
20. Fregolente, L.G.; dos Santos, J.V.; Vinci, G.; Piccolo, A.; Moreira, A.B.; Ferreira, O.P.; Bisinoti, M.C.; Spaccini, R. Insights on molecular characteristics of hydrochars by ^{13}C-NMR and off-line TMAH-GC/MS and assessment of their potential use as plant growth promoters. *Molecules* **2021**, *26*, 1026. [CrossRef]
21. Cao, X.; Ro, K.S.; Libra, J.A.; Kammann, C.I.; Lima, I.; Berge, N.; Li, L.; Li, Y.; Chen, N.; Yang, J.; et al. Effects of biomass types and carbonization conditions on the chemical characteristics of hydrochars. *J. Agric. Food Chem.* **2013**, *61*, 9401–9411. [CrossRef] [PubMed]
22. Geppi, M.; Forte, C. The SPORT-NMR software: A tool for determining relaxation times in unresolved NMR spectra. *J. Magn. Reson.* **1999**, *137*, 177–185. [CrossRef] [PubMed]
23. Smernik, R.J.; Eckmeier, E.; Schmidt, M.W.I. Comparison of solid-state C-13 NMR spectra of soil organic matter from an experimental burning site acquired at two field strengths. *Aust. J. Soil Res.* **2008**, *46*, 122–127. [CrossRef]
24. Poletto, M.; Zattera, A.J.; Santana, R.M.C. Structural differences between wood species: Evidence from chemical composition, FTIR spectroscopy, and thermogravimetric analysis. *J. Appl. Polym. Sci.* **2012**, *126*, E337–E344. [CrossRef]
25. Schwanninger, M.; Rodrigues, J.C.; Pereira, H.; Hinterstoisser, B. Effects of short-time vibratory ball milling on the shape of FT-IR spectra of wood and cellulose. *Vib. Spectrosc.* **2004**, *36*, 23–40. [CrossRef]
26. Sharma, R.K.; Wooten, J.B.; Baliga, V.L.; Lin, X.; Chan, W.G.; Hajaligol, M.R. Characterization of chars from pyrolysis of lignin. *Fuel* **2004**, *83*, 1469–1482. [CrossRef]
27. Keiluweit, M.; Nico, P.S.; Johnson, M.G.; Kleber, M. Dynamic molecular structure of plant biomass-derived black carbon (Biochar). *Environ. Sci. Technol.* **2010**, *44*, 1247–1253. [CrossRef]
28. Sevilla, M.; Maciá-Agulló, J.A.; Fuertes, A.B. Hydrothermal carbonization of biomass as a route for the sequestration of CO_2: Chemical and structural properties of the carbonized products. *Biomass Bioenergy* **2011**, *35*, 3152–3159. [CrossRef]
29. Lammers, K.; Arbuckle-Keil, G.; Dighton, J. FT-IR study of the changes in carbohydrate chemistry of three New Jersey pine barrens leaf litters during simulated control burning. *Soil Biol. Biochem.* **2009**, *41*, 340–347. [CrossRef]

30. Kloss, S.; Zehetner, F.; Dellantonio, A.; Hamid, R.; Ottner, F.; Liedtke, V.; Schwanninger, M.; Gerzabek, M.H.; Soja, G. Characterization of slow pyrolysis biochars: Effects of feedstocks and pyrolysis temperature on biochar properties. *J. Environ. Qual.* **2012**, *41*, 990–1000. [CrossRef] [PubMed]
31. Liu, Z.; Quek, A.; Hoekman, S.K.; Balasubramanian, R. Production of solid biochar fuel from waste biomass by hydrothermal carbonization. *Fuel* **2013**, *103*, 943–949. [CrossRef]
32. Hu, J.; Shen, D.; Wu, S.; Zhang, H.; Xiao, R. Effect of temperature on structure evolution in char from hydrothermal degradation of lignin. *J. Anal. Appl. Pyrolysis* **2014**, *106*, 118–124. [CrossRef]
33. Budai, A.; Calucci, L.; Rasse, D.P.; Tau Strand, L.; Pengerud, A.; Wiedemeier, D.; Abiven, S.; Forte, C. Effects of pyrolysis conditions on Miscanthus and corncob chars: Characterization by IR, solid state NMR and BPCA analysis. *J. Anal. Appl. Pyrolysis* **2017**, *128*, 335–345. [CrossRef]
34. Adapa, P.K.; Tabil, L.G.; Schoenau, G.J.; Canam, T.; Dumonceaux, T. Quantitative analysis of lignocellulosic components of non-treated and steam exploded barley, canola, oat and wheat straw using Fourier transform infrared spectroscopy. *J. Agric. Sci. Technol. B* **2011**, *1*, 177–188.
35. Chen, B.; Zhou, D.; Zhu, L. Transitional adsorption and partition of nonpolar and polar aromatic contaminants by biochars of pine needles with different pyrolytic temperatures. *Environ. Sci. Technol.* **2008**, *42*, 5137–5143. [CrossRef] [PubMed]
36. Zhang, M.; Yang, H.; Liu, Y.; Sun, X.; Zhang, D.; Xue, D. First identification of primary nanoparticles in the aggregation of HMF. *Nanoscale Res. Lett.* **2012**, *7*, 38. [CrossRef]
37. He, Q.; Cheng, C.; Raheem, A.; Ding, L.; Shiung Lam, S.; Yu, G. Effect of hydrothermal carbonization on woody biomass: From structure to reactivity. *Fuel* **2022**, *330*, 125586. [CrossRef]
38. Volpe, M.; Wüst, D.; Merzari, F.; Lucian, M.; Andreottola, G.; Kruse, A.; Fiori, L. One stage olive mill waste streams valorisation via hydrothermal carbonization. *Waste Manag.* **2018**, *20*, 224–234. [CrossRef]
39. Kolodziejski, W.; Frye, J.S.; Maciel, G.E. Carbon-13 nuclear magnetic resonance spectrometry with cross polarization and magic-angle spinning for analysis of lodgepole pine wood. *Anal. Chem.* **1982**, *54*, 1419–1424. [CrossRef]
40. Haw, J.F.; Maciel, G.E.; Schroeder, H.A. Carbon-13 nuclear magnetic resonance spectrometric study of wood and wood pulping with cross polarization and magic-angle spinning. *Anal. Chem.* **1984**, *56*, 1323–1329. [CrossRef]
41. Bardet, M.; Emsley, L.; Vincendon, M. Two-dimensional spin-exchange solid-state NMR studies of ^{13}C-enriched wood. *Solid State Nucl. Magn. Reson.* **1997**, *8*, 25–32. [CrossRef] [PubMed]
42. Czimczik, C.I.; Preston, C.M.; Schmidt, M.W.I.; Werner, R.A.; Schulze, E.-D. Effects of charring on mass, organic carbon, and stable carbon isotope composition of wood. *Org. Geochem.* **2002**, *33*, 1207–1223. [CrossRef]
43. Atalla, R.H.; VanderHart, D.L. The role of solid state ^{13}C NMR spectroscopy in studies of the nature of native celluloses. *Solid State Nucl. Magn. Reson.* **1999**, *15*, 1–19. [CrossRef] [PubMed]
44. Lüdemann, H.-D.; Nimz, H. Carbon-13 nuclear magnetic resonance spectra of lignins. *Biochem. Biophys. Res. Commun.* **1973**, *52*, 1162–1169. [CrossRef] [PubMed]
45. Schaefer, J.; Sefcik, M.D.; Stejskal, E.O.; McKay, R.A.; Hall, P.L. Characterization of the catabolic transformation of lignin in culture by magic-angle carbon-13 nuclear magnetic resonance. *Macromolecules* **1981**, *14*, 557–559. [CrossRef]
46. Hatfield, G.R.; Maciel, G.E.; Erbatur, O.; Erbatur, G. Qualitative and quantitative analysis of solid lignin samples by carbon-13 nuclear magnetic resonance spectrometry. *Anal. Chem.* **1987**, *59*, 172–179. [CrossRef]
47. Hatcher, P.G. Chemical structural studies of natural lignin by dipolar dephasing solid-state ^{13}C nuclear magnetic resonance. *Org. Geochem.* **1987**, *11*, 31–39. [CrossRef]
48. Mao, J.; Holtman, K.M.; Scott, J.T.; Kadla, J.F.; Schmidt-Rohr, K. Differences between lignin in unprocessed wood, milled wood, mutant wood, and extracted lignin detected by ^{13}C solid-state NMR. *J. Agric. Food Chem.* **2006**, *54*, 9677–9686. [CrossRef]
49. Teerman, S.C.; Hwang, R.J. Evaluation of the liquid hydrocarbon potential of coal by artificial maturation techniques. *Org. Geochem.* **1991**, *17*, 749–764. [CrossRef]
50. Mao, J.-D.; Schmidt-Rohr, K. Recoupled long-range C-H dipolar dephasing in solid-state NMR, and its use for spectral selection of fused aromatic rings. *J. Magn. Reson.* **2003**, *162*, 217–227. [CrossRef]
51. Baccile, N.; Laurent, G.; Babonneau, F.; Fayon, F.; Titirici, M.-M.; Antonietti, M. Structural characterization of hydrothermal carbon spheres by advanced solid-state MAS ^{13}C NMR investigations. *J. Phys. Chem. C* **2009**, *113*, 9644–9654. [CrossRef]
52. Falco, C.; Caballero, F.P.; Babonneau, F.; Gervais, C.; Laurent, G.; Titirici, M.-M.; Baccile, N. Hydrothermal carbon from biomass: Structural differences between hydrothermal and pyrolyzed carbons via ^{13}C solid state NMR. *Langmuir* **2011**, *27*, 14460–14471. [CrossRef] [PubMed]
53. Lu, X.; Pellechia, P.J.; Flora, J.R.V.; Berge, N.D. Influence of reaction time and temperature on product formation and characteristics associated with the hydrothermal carbonization of cellulose. *Bioresour. Technol.* **2013**, *138*, 180–190. [CrossRef] [PubMed]
54. Bobleter, O. Hydrothermal degradation of polymers derived from plants. *Prog. Polym. Sci.* **1994**, *19*, 797–841. [CrossRef]
55. Mok, W.S.-L.; Antal, M.J., Jr. Uncatalyzed solvolysis of whole biomass hemicellulose by hot compressed liquid water. *Ind. Eng. Chem. Res.* **1992**, *31*, 1157–1161. [CrossRef]
56. Lei, Y.; Su, H.; Tianc, R. Morphology evolution, formation mechanism and adsorption properties of hydrochars prepared by hydrothermal carbonization of corn stalk. *RSC Adv.* **2016**, *6*, 107829. [CrossRef]
57. Hashaikeh, R.; Fang, Z.; Butler, I.S.; Hawari, J.; Kozinski, J.A. Hydrothermal dissolution of willow in hot compressed water as a model for biomass conversion. *Fuel* **2007**, *86*, 1614–1622. [CrossRef]

58. Falco, C.; Baccile, N.; Titirici, M.-M. Morphological and structural differences between glucose, cellulose and lignocellulosic biomass derived hydrothermal carbons. *Green Chem.* **2011**, *13*, 3273–3281. [CrossRef]
59. Dinjus, E.; Kruse, A.; Tröger, N. Hydrothermal carbonization—1. Influence of lignin in lignocelluloses. *Chem. Eng. Technol.* **2011**, *34*, 2037–2043. [CrossRef]
60. Zawadzki, J.; Wisniewski, M. ^{13}C NMR study of cellulose thermal treatment. *J. Anal. Appl. Pyrolysis* **2002**, *62*, 111–121. [CrossRef]
61. Yu, L.; Falco, C.; Weber, J.; White, R.J.; Howe, J.Y.; Titirici, M.-M. Carbohydrate-derived hydrothermal carbons: A thorough characterization study. *Langmuir* **2012**, *28*, 12373–12383. [CrossRef] [PubMed]
62. Peterson, A.A.; Vogel, F.; Lachance, R.P.; Fröling, M.; Antal, M.J., Jr.; Tester, J.W. Thermochemical biofuel production in hydrothermal media: A review of sub- and supercritical water technologies. *Energy Environ. Sci.* **2008**, *1*, 32–65. [CrossRef]